REVERSE MONTE CARLO REFINEMENT OF DISORDERED SILICA PHASES

David A. Keen

ISIS Facility
Rutherford Appleton Laboratory
Chilton, Didcot
OxonOXll 0QX
U. K.

INTRODUCTION

This chapter will provide a detailed description of the reverse Monte Carlo (RMC) modelling method. RMC has been established over the last ten years as a general method for obtaining models of a wide variety of disordered structures, including liquids, glasses, crystals, polymers and amorphous magnets. Particular emphasis will be given here on how it may be used to refine the disorder in glassy and crystalline materials. In addition to explaining the principles and rationale of the RMC method, results from modelling various polymorphs of silica will be used to demonstrate how the method works in practice. For the crystalline systems, the RMC models will be compared to diffraction patterns from powdered samples, since RMC modelling of single crystal diffraction is covered in the chapter by V. M. Nield in this volume.

The outline of this chapter is as follows. The next section introduces various background formulae which underpin the ideas of total scattering. Then reverse Monte Carlo modelling is introduced and described in detail. This is followed by a section which works through the application of RMC *modelling* to the structure of glassy silica and the results are compared with other existing models. The ideas of RMC *refinement* are then described and applied to glassy silica. Preliminary results from RMC refinement of disordered crystalline phases of silica are then described. Finally, conclusions are made with a discussion of future possibilities for the RMC method.

THEORETICAL FORMALISM

Before describing the modelling method in detail, it is necessary to define various relevant correlation functions. The data used to constrain the RMC models described in this chapter are from 'total scattering' measurements. The ideal total scattering

Local Structure from Diffraction
Edited by S.J.L Billinge and M.F. Thorpe, Plenum Press, New York, 1998

measurement would collect scattering over all momentum transfers $0<|\boldsymbol{Q}|<\infty$, integrating at each $|\boldsymbol{Q}|$ over all possible enegy transfers which may take place within the sample. Most good neutron and X-ray diffraction measurements are a reasonable approximation to this ideal, albeit with a reduced range of $|\boldsymbol{Q}|$. Total scattering therefore contains both Bragg and diffuse components from a crystalline material and, as will be shown later, it is vital to include the diffuse scattering when considering structural disorder. The total structure factor, *F(Q),* obtained from careful correction of neutron total scattering data[1] from an *n*-component system, can be defined in terms of Faber-Ziman partial structure factors $A_{\alpha\beta}(Q)$.[2]

$$F(Q) = \sum_{\alpha=1}^{n}\sum_{\beta=1}^{n} c_\alpha c_\beta \bar{b}_\alpha \bar{b}_\beta [A_{\alpha\beta}(Q) - 1] \tag{1}$$

where $\bar{b}_\alpha$ and c_α is the coherent neutron scattering length and proportion of atom α respectively. The formula still holds for X-ray scattering if the neutron scattering lengths are replaced by X-ray form factors. These partial structure factors are the sine Fourier transforms of the partial radial distribution functions, $g_{\alpha\beta}(r)$

$$g_{\alpha\beta}(r) - 1 = \frac{1}{(2\pi)^3 \rho}\int_0^\infty 4\pi Q^2 [A_{\alpha\beta}(Q) - 1]\frac{\sin(Qr)}{Qr} \mathrm{d}Q \tag{2}$$

where ρ is the number density of atoms. $g_{\alpha\beta}(r)$ are defined explicity as

$$g_{\alpha\beta}(r) = \frac{n_{\alpha\beta}(r)}{4\pi r^2 \mathrm{d}r \rho_\beta} \tag{3}$$

where $n_{\alpha\beta}(r)$ is the number of particles of type β between distances r and $r+dr$ from a particle of type α, averaged over all particles α. ρ_β is the number density of atom type β. It is also useful to define a total radial distribution function $G'(r)$ in terms of $g_{\alpha\beta}(r)$

$$G'(r) = \sum_{\alpha=1}^{n}\sum_{\beta=1}^{n} c_\alpha c_\beta \bar{b}_\alpha \bar{b}_\beta [g_{\alpha\beta}(r) - 1] \tag{4}$$

such that the total structure factor $F(Q)$ is the sine Fourier transform of $G'(r)$:

$$F(Q) = \rho\int_0^\infty 4\pi r^2 G'(r)\frac{\sin(Qr)}{Qr} \mathrm{d}Q \tag{5}$$

Frequently $G(r)$ is used, which is a normalised total radial distribution function

$$G(r) - 1 = G'(r) / \sum_{\alpha=1}^{n} c_\alpha \bar{b}_\alpha \tag{6}$$

such that $G(r\rightarrow\infty)=1$ and $G(r<r_0)=0$, where r_0 is the smallest distance two atoms may approach each other. *T(r),* another popular form of the real space correlation function, is then proportional to *rG(r).*

$n_{\alpha\beta}(r)$ may be calculated simply from a three-dimensional configuration of atom positions and from these functions all the above functions may be derived. Similarly *F(Q),* the coherent part of the experimental total scattering can be used either directly, or Fourier transformed to *G(r)* for comparison with the equivalent functions from the computer generated models.

REVERSE MONTE CARLO MODELLING

Background

The reverse Monte Carlo modelling technique was developed to create three-dimensional structural models of liquid and amorphous (or glassy) materials *without bias.* Liquids and glasses are, in general, macroscopically isotropic and in a diffraction measurement the material will scatter isotropically, varying only as a function of the modulus of the momentum transfer, $|\boldsymbol{Q}|$. Such a one-dimensional scattering function (the structure factor *F(Q)* - see Equation 1) can be Fourier transformed to provide information about atom-atom distances, but vector information is lost.

Modelling of some form or another was one obvious way to attempt a reconstruction of the three-dimensional local structure of glasses and liquids from the one-dimensional scattering information. The earliest attempts along these lines were by Kaplow *et al* [3] in 1968 (investigating vitreous selenium) and Renninger *et al* [4] in 1974 (on arsenic-selenium glasses). Both these works used small spherical models and further progress was hampered by the limitations in computer power. Subsequently the concepts were developed successfully by McGreevy and Pusztai[5] who modelled the structure of liquid argon in 1988, coined the term 'reverse Monte Carlo modelling' and established the basic method which is used extensively today . McGreevy and Pusztai argued[5] that the RMC method's strength lay in the fact that no interatomic potentials were imposed on the structural model and hence the technique was very different from the more familiar Monte Carlo simulation which uses a set of potentials to constrain the model. In RMC modelling, the model is only required to agree with the structural data. It was believed that, in principle, the resultant RMC models could then be used to determine the interatomic potentials which governed the structure. Instead of working from the potentials to the structure to the structural data, the structural data were used to determine the structure and hence the potentials. The Monte Carlo cycle was operated in 'reverse'. However, because the available structural data do not necessarily describe a unique structure (see later) and three-body terms (which are not contained in the structure factor *F(Q))* are equally important in determining structure, in practice it is very difficult to use RMC to determine appropriate potential functions.

The RMC approach has many advantages over other modelling techniques, principally because it does not bias the resulting model. If the data do not require a specific structural feature, then the RMC model is unlikely to show such a feature. This has to some extent changed the way that disordered structures, and liquid and amorphous structures in particular, are considered. The local structure of a glass is usually thought of in terms of small structural units which are found in chemically similar crystalline materials. Models are then built by joining these semi-rigid structural units, either explicitly or implicitly from the description of interatomic potential functions. This can result in models which are too ordered and do not have sufficient flexibility to include other possible structural motifs. In contrast, no such features are assumed in RMC models and often exactly the opposite type of structural models are obtained with too much disorder. As will be shown later, this is because the data do not provide sufficient structural information to define uniquely the

structure and a disordered structure, although consistent with the data, is more likely to result from random Monte Carlo moves. For many systems neither extreme is entirely satisfactory and a middle ground must be established. As a result, although RMC is a very powerful method, it must be controlled in appropriate ways to yield good, respresentative structural models. Such control can be achieved by using a constrained RMC *refinement* of a carefully constructed structural model which already contains pertinent structural features. Thus the best features of RMC modelling (lack of bias, structural flexibility, consistency with experimental data) are combined with an initial model containing structural elements which RMC modelling may not be good at reproducing, but are nonetheless indisputable. This is clearly common sense when considering disordered crystals, since the long-range periodicity and average crystal structure must be maintained throughout the RMC modelling of the short-range structural disorder. This is analogous to the process of Rietveld refinement[7], where an initial structural model is refined by comparison with a powder diffraction pattern.

The RMC Modelling Method

1. Generate a three-dimensional configuration of N atoms, which is constrained by periodic boundary conditions. The configuration is frequently a cube with lengths L for convenience, but can have different geometries to suit (for example) different crystal symmetries. The practical effect of periodic boundary conditions is that when an atom is moved beyond one side of the configuration box, it moves back into the box at the opposite side. All atoms within the configuration must also satisfy 'closest approach' constraints such that two atom types may only come within a certain distance of each other. The closest approaches may, with ideal data, be determined uniquely from the partial radial distribution functions, but they are more likely to be deduced from a combination of factors, and can be adjusted from examination of how the modelling progresses. It is important at the outset to make them smaller than may seem physical, since they act as an infinite hard-core potential.

2. Calculate the function corresponding to the experimentally determined data, such as the total structure factor $F(Q)$

3. Calculate the difference between the measured structure factor $F_{\mathrm{expt}}(Q)$ and that determined from the configuration $F_{\mathrm{calc}}(Q)$.

$$\chi^2_{\mathrm{old}} = \sum_{i=1}^{n} [F_{\mathrm{calc}}(Q_i)_{\mathrm{old}} - F_{\mathrm{expt}}(Q_i)]^2 / \sigma(Q_i)^2 \qquad (7)$$

   where the sum is over all n experimental data points, each with error $\sigma(Q_i)$.

4. One atom is selected at random

5. This atom is moved a random amount in a random direction up to a pre-defined limit. If the atom still satisfies the closest approach constraints, the experimentally determined data is recalculated (e.g. $F_{\mathrm{calc}}(Q)_{\mathrm{new}}$). Since only one atom is moved at any one time, it is only necessary to calculate the change in $F_{\mathrm{calc}}(Q)$ due to the atom's move. This involves a calculation of size $\sim N$ compared with $\sim N^2$ for calculating $F_{\mathrm{calc}}(Q)$ from scratch at each iteration.

6. The experimentally determined data are compared.

$$\chi^2_{new} = \sum_{i=1}^{n} [F_{calc}(Q_i)_{new} - F_{expt}(Q_i)]^2 / \sigma(Q_i)^2 \quad (8)$$

If the new χ^2 is lower than the one determined with the atom in the previous position, $\chi^2_{new} < \chi^2_{old}$, the move it accepted and the new configuration becomes the old configuration. If the new χ^2 is higher then the move is accepted with probability $P = \exp(-(\chi^2_{new} - \chi^2_{old})/2)$ or else it is rejected. In practice the acceptance is determined by comparing P with a random number R between 0 and 1 generated by the computer. The move is accepted when $P > R$.

7. The algorithm is continued by returning to step 4. Initially χ^2 will decrease until it reaches an equilibrium value and further moves make little change to χ^2. The model is then said to have converged. Moves may then be continued and configurations collected every ~N accepted moves to collect statistically independent configurations.

As can be seen from the description given above, RMC modelling and the well known Metropolis Monte Carlo simulation[8] are very similar. The only difference is that whereas Monte Carlo simulation samples the potential energy, RMC samples the difference between calculated and experimental structural data. The attributes that are particularly important in the Monte Carlo algorithm[9] should be replicated in the RMC algorithm. The most important of which is the use of a Markov chain, so that local minima are avoided and the final configuration is independent of the starting point.

The definition of χ^2 may be generalised to include comparison with extra data sets such as X-ray, neutron and EXAFS structure factors. Equally extra terms may be introduced to constrain the RMC model further such as predefined atom-atom co-ordinations or nearest neighbour distances. χ^2 may then be written as

$$\chi^2 = \sum_{k} \sum_{i=1}^{n} [F_{calc}(Q_i)_k - F_{expt}(Q_i)_k]^2 / \sigma_k(Q_i)^2 + \sum_{j=1}^{m} (f_j^{req} - f_j^{RMC})^2 / \sigma_j^2 \quad (9)$$

to include comparison with the k structure factors and the m constraints. f^{req} and f^{RMC} are the required value of the constraint and the value calculated from the RMC generated configuration respectively. σ_j is a weighting term which influences the strength of any particular constraint. In a crude manner co-ordination constraints can be considered as simple three-body terms restraining the model. In crystalline materials it is particularly necessary to constrain the model, for example to maintain the integrity of a molecular fragment or to restrict a molecule to a finite number of possible orientations and these can simply be included in the definition of χ^2 (Equation 9). Equally the model may be constrained by restricting the movements of atoms to specific regions of the configuration, such as disordering an atom along a specific direction, only allowing atoms to swap etc.

The ability to fit different data sets with the same three-dimensional model is particularly important in order to separate the contributions from different partial radial distribution functions. As shown in Equation 1, the total structure factor $F(Q)$ for an n component system is composed of a weighted sum of $\frac{1}{2}n(n+1)$ partial structure factors $A_{\alpha\beta}(Q)$. Therefore $F(Q)$ from a two component system is composed of three partial structure factors or, via Equation 2, three partial radial distribution functions, $g_{\alpha\beta}(r)$. The

technique of neutron isotopic substitution[10] can be used to obtain $g_{\alpha\beta}(r)$ experimentally, where, for an n component system, $\frac{1}{2}n(n+1)$ total structure factors $F(Q)$ composed of different weightings (obtained by using different isotopes of the same element with different neutron scattering lengths) of the same partial structure factors, $A_{\alpha\beta}(Q)$, are measured. $g_{\alpha\beta}(r)$ are then obtained by simultaneously solving the set of $F(Q)$ for $A_{\alpha\beta}(Q)$. Even given that suitable isotopes exist for the system of interest, the errors in measurement may mean that the results from such a separation may not provide $g_{\alpha\beta}(r)$ which are self-consistent. The combination of neutron and X-ray $F(Q)$ may provide partial separation of $A_{\alpha\beta}(Q)$, but it can never be unambiguous, even for a binary compound. RMC modelling of the data compensates in part for this loss of information since the $g_{\alpha\beta}(r)$, which come from a single three-dimensional configuration, must be self-consistent. It should however be stressed that the better the data, the more constrained the final model will be and to get the best from RMC modelling, high quality data are required.

MODELLING GLASSY SILICA, SiO_2

Previous Models of Glassy Silica

It was realised very early that glassy materials, although highly disordered and isotropic over large distances, may possess a definite local order. Zachariasen[11] first introduced the idea of a continuous random network (CRN) for a glassy structure where the atoms are bonded locally and form a three-dimensional structure with no periodicity or symmetry. Based on the CRN model, glassy silica SiO_2 is thought of as a continuous network of SiO_4 units joined at the corners such that each Si is surrounded by four O and each O has two Si neighbours. Given that in most silicate crystals the SiO_4 unit forms an approximate tetrahedron, then a single Si-O bond length and O-Si-O bond angle of 109.47° would be expected in the glass. This is supported by the experimental neutron $G(r)$ which has one strong peak at 1.617Å (Si-O) and a second one at 2.626Å (O-O) implying a O-Si-O average angle of 108.6°.[12] Also NMR experiments find little evidence for the Si co-ordination to be different from 4 or the O co-ordination to be different from 2.[13] However the manner in which these SiO_4 units are joined is more difficult to obtain directly from experimental data. Steric constraints prevent face- or edge-sharing tetrahedra so all SiO_4 tetrahedra must be corner-sharing, described by three angles, the Si-O-Si bond angle and two torsional angles which define the orientation of each joined tetrahedra about the Si-O bonds which meet at the common O atom (see Figure 1). The first (Si-O) and third (Si-Si) lowest r peaks in $G(r)$ would give an average value of the Si-O-Si bond angle, but the Si-Si peak is partially overlapped and very weak in the neutron $G(r)$. Synchrotron X-ray data have been used to deduce a broad Si-O-Si bond angle (α) distribution, $V(\alpha)=V_1(\alpha)\sin\alpha$ with V peaking at 143° and V_1 at 180°.[14] Longer-range structure is virtually impossible to extract directly from structural data (apart from the characteristic atom-atom distances). It is therefore not entirely surprising that modelling has been used to investigate the structure of silica further, given that direct experimental information about the structure becomes vague even at distances ~3Å and greater and that it is these distances which play the most important part in glass formation.

One of the earliest three-dimensional models of silica glass was hand-built by Bell and Dean[15]. Such models were in reasonable agreement with the then available diffraction data but were tedious to construct and the density was difficult to control, being critically dependent on the chosen Si-O-Si bond angles. Subsequent models were all computer generated, the most comprehensive of which were by Gladden[16] who followed a complex

recipe forjoining SiO_4 units to construct 1000 atom clusters. Some of her models had very good agreement with $G(r)$ and could be used to investigate optimal Si-O-Si bond angle distributions and longer-range structure. The other method which has been used extensively is Molecular Dynamics simulation[17]. These simulations vary in configuration size and simulation complexity, but do not, in general, fit the diffraction data as well as the empirical models.

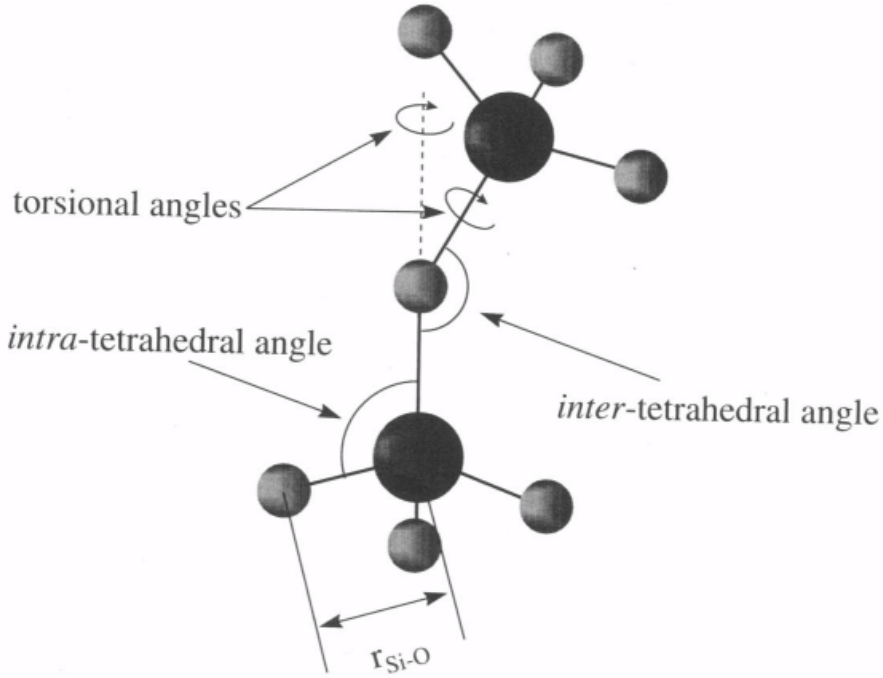

Figure 1. Schematic diagram showing the most likely bonding mechanism in glassy silica where two SiO_4 tetrahedral units are joined at a common oxygen atom.

RMC Models of Glassy Silica

For SiO_2, it is not possible to experimentally separate the Si-Si, Si-O and O-O partial correlation functions, since suitable isotopes for isotopic substitution do not exist and the two available $F(Q)$ (X-ray and neutron) are not sufficient to obtain three $A_{\alpha\beta}(Q)$. The first RMC model of silica[18] used the method in its basic, unconstrained form starting from a configuration of 2596 atoms randomly placed in a cubic configuration box of length 34.017Å. Good agreement was obtained with the X-ray and neutron $F(Q)$ but the partial radial distribution functions $g_{\alpha\beta}(r)$ contained some unsatisfactory features which suggested that the separation of the $g_{\alpha\beta}(r)$ was not correct (for example there was a weak peak in $g_{Si\text{-}O}(r)$ at r values where an Si-O correlation was unlikely and which could instead be attributed to the strongest peak in $g_{O\text{-}O}(r)$). Also, the average Si-O co-ordination was only 3.7 and the average O-Si co-ordination was 1.8 and some of the SiO_4 tetrahedral unit were somewhat distorted. The O-Si-O bond angle distribution peaked sharply at 109.6°, but contained a significant tail to higher angles. It is perhaps more significant, given the random starting configuration and lack of any constraints, that any identifiable structural features were found and in fact the majority of the configuration contained joined and structurally correct SiO_4 units. However, some regions of the configuration did not possess the required local connected structure and the RMC modelling was not able to completely connect the structure unaided, since it could find a less-well connected structure with suitable agreement to the data.

Subsequent to this model, a constrained RMC model of 3000 atoms was produced[19], requiring the model to maintain the expected Si-O and O-Si co-ordinations within a defined near-neighbour distance and still fit the data. The second summation term in Equation (9) was used whereby there was a penalty in the χ^2 for all non-perfectly co-ordinated atoms. Again good fits to the *F(Q)* data were obtained (see Figure 2) and 96.2% of the Si atoms were co-ordinated to four O atoms and 95.4% of the O atoms were co-ordinated to two Si atoms. However, the good connectivity of this model was achieved at the expense of the local order, with, if anything, more distorted SiO_4 tetrahedra than the unconstrained model (including a weak peak on the high-*r* side of the low-*r* Si-O peak). Although both these models have considerable merit, they are both flawed in some important respects.

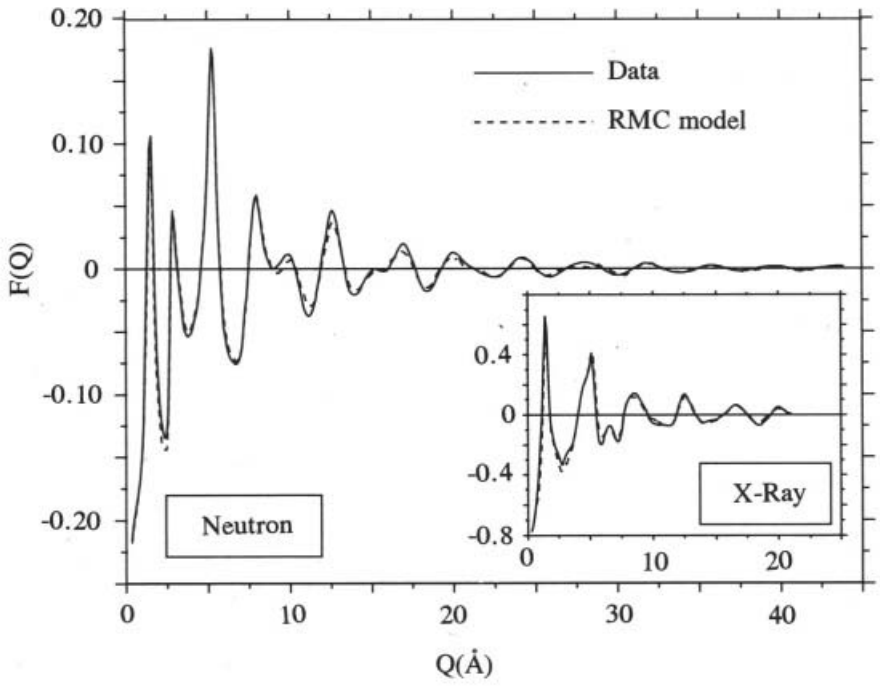

Figure 2. Structure factors for glassy silica calculated from the RMC model of Wicks[19] with co-ordination constraints (dashed lines) compared with those obtained by experiment - neutron[12] and X-ray[20] (inset).

REVERSE MONTE CARLO REFINEMENT

The flaws in the RMC models of glassy silica which have been pointed out in the above section should not be used to discount the RMC modelling method completely. It should be remembered that it was the intention of RMC modelling at the outset to produce valid three-dimensional structural models without bias. The RMC models have demonstrated that the data do indeed suggest that silica glass is composed of ideally connected edge-sharing SiO_4 tetrahedra and they have been used to quantify the Si-O-Si bond angle distribution and further details of the structure. However RMC modelling of the data alone will not be sufficient to produce a model which displays these structural characteristics perfectly. RMC modelling tends to produce the most disordered structure which is consistent with the data and such a model will not produce a glass structure which is composed of very specific structural units. It is therefore necessary to introduce extra constraints into the model in a satisfactory manner without unduly prejudicing the final structure. The constrained model[19] imposed connectivity at the expense of increased SiO_4 tetrahedral distortion.

The two-stage process of RMC *refinement* has therefore been developed[21]. A starting model is created independent of the data which possesses the characteristics which are unambiguously known to be correct and the data are then used to refine the model with RMC. It is clearly essential to constrain the RMC refinement in a suitable way so as not to destroy the essential structural features of the initial model whilst allowing the refinement sufficient flexibility to fit the data. In the case of a glass structure this would usually mean that the initial model had the correct local structure and the RMC refined final model was then used to investigate longer-range structure and amount of distortion. For a disordered crystal, the initial model would normally be the average crystal structure deduced from the analysis of the Bragg peaks and the RMC refined model would provide details about the local deviations from the average structure.

RMC Refinement of Glassy Silica

A form of this method was attempted by Gladden[22] starting from her existing models and Bionducci *et al* [23] attempted to obtain a model of glassy silica starting from the α-quartz structure. However neither of these models started with a completely connected CRN and periodic boundary conditions and during RMC refinement their models were corrupted such that the atoms in Gladden's cluster became too close to each other and the connectivity initially present in α-quartz was partially destroyed.

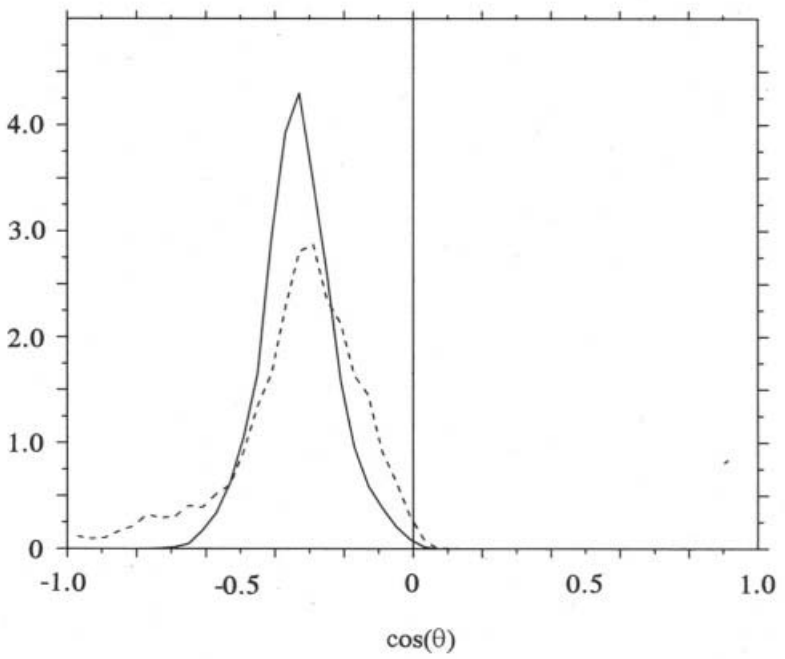

Figure 3. The intra-tetrahedral O-Si-O bond angle distribution from the RMC co-ordination constrained model of Wicks[19] (dashed line) compared with the initial model used for RMC refinement[21] (full line) (arbitrary units).

The most recent RMC refinement of glassy silica starts from a model of 3000 atoms and periodic boundary conditions[21]. The initial model and the method of its construction has already been described[21]. This model has a similar connectivity to the model described by Wicks[19], but has the advantage that the SiO_4 tetrahedra are not distorted (see Figure 3). The *F(Q)* calculated from this starting model are actually in good agreement with the experimental data except that they do not reproduce the intensity of the peak at lowest *Q* well. This model was then refined using RMC by slowly increasing the weighting of the

X-ray and neutron *F(Q)* with respect to the following constraints designed to maintain the integrity of the SiO_4 tetrahedra (compare with Equation 9):

$$\sum (r_{Si-O} - R_{Si-O})^2 / \sigma_{Si-O} + \sum (\theta_{O-Si-O} - \Theta_{O-Si-O})^2 / \sigma_{O-Si-O} \qquad (10)$$

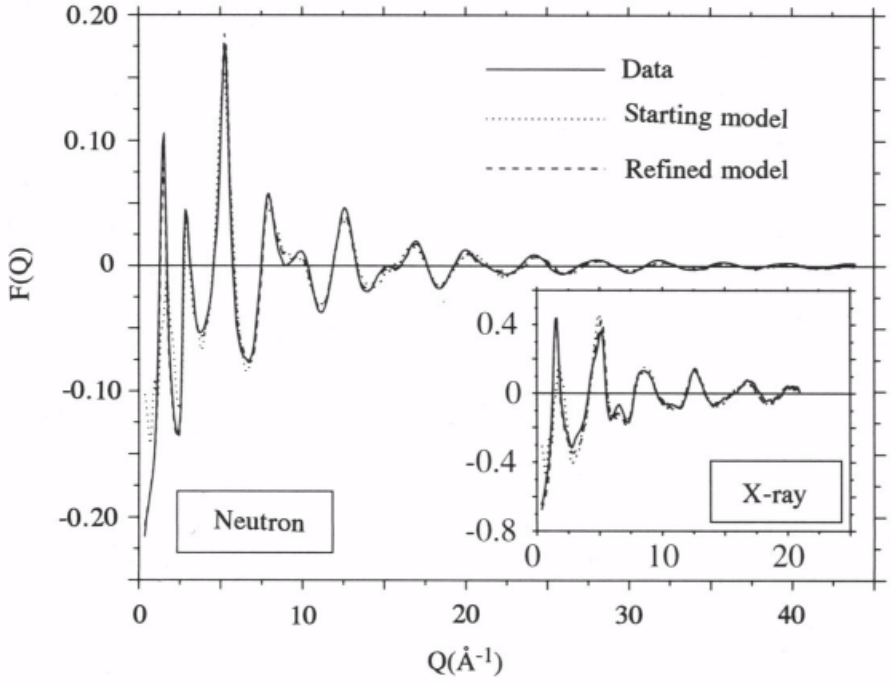

Figure 4. Structure factors for glassy silica calculated from the starting model (dotted line), the RMC refined model[21] (dashed lines) compared with those obtained by experiment - neutron[12] and X-ray[14] (inset).

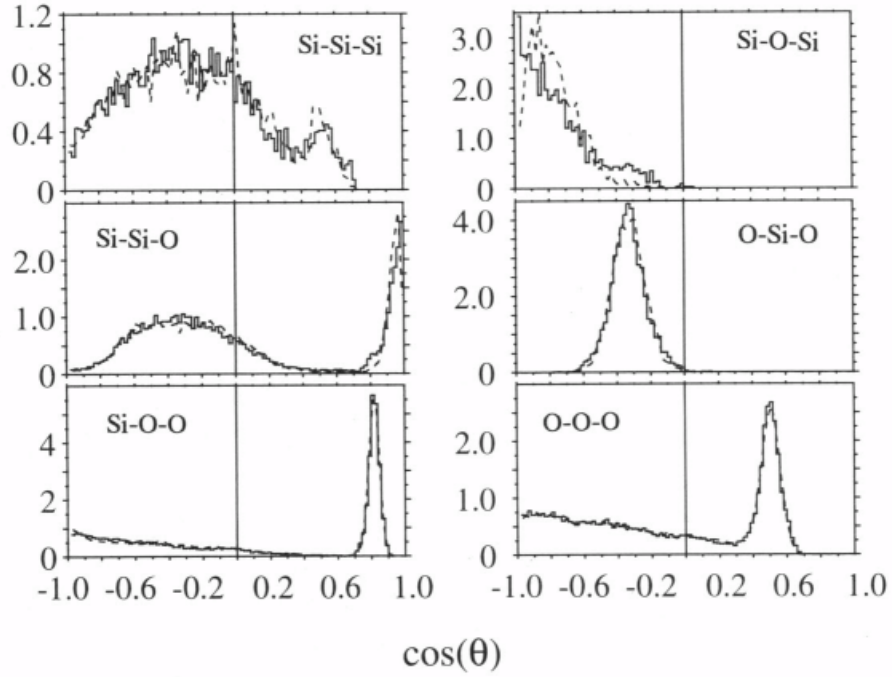

Figure 5. Bond angle distributions for glassy silica calculated from the starting model (dashed line) and the RMC refined model (full line)[21] (arbitrary units).

where $R_{Si\text{-}O}$ is the ideal Si-O distance (1.61 Å) and $\Theta_{O\text{-}Si\text{-}O}$ is the ideal tetrahedral angle, with $\sigma_{Si\text{-}O}$ and $\sigma_{O\text{-}Si\text{-}O}$ chosen to produce qualitatively the appropriate widths of the two lowest-*r* peaks in *G(r)*. The connectivity was also maintained by not allowing atoms to pass past each other - the CRN could deform but Si-O bonds could not be broken. The model produced in this way gave excellent agreement with the *F(Q)*'s, better agreement than the previous RMC models, with the first structure factor peak fitting well (see Figure 4). There is not much change in the $g_{\alpha\beta}(r)$'s after RMC refinement, with most of the changes in the longer-range details (as reflected by the changes in the first structure factor peak). The most significant difference is found in the Si-O-Si bond angle distribution which becomes broader on RMC refinement (Figure 5).

This RMC refinement of glassy silica demonstrates that it is possible to use RMC modelling, suitably constrained, to improve the fit to data without breaking up an existing structure. The development from the earlier RMC models, which showed that certain structural units are in the glass structure, to the subsequent RMC refinement of a model which set out to incorporate such units, with an improved fit to the data, is a powerful and potentially wide-ranging application of the RMC technique.

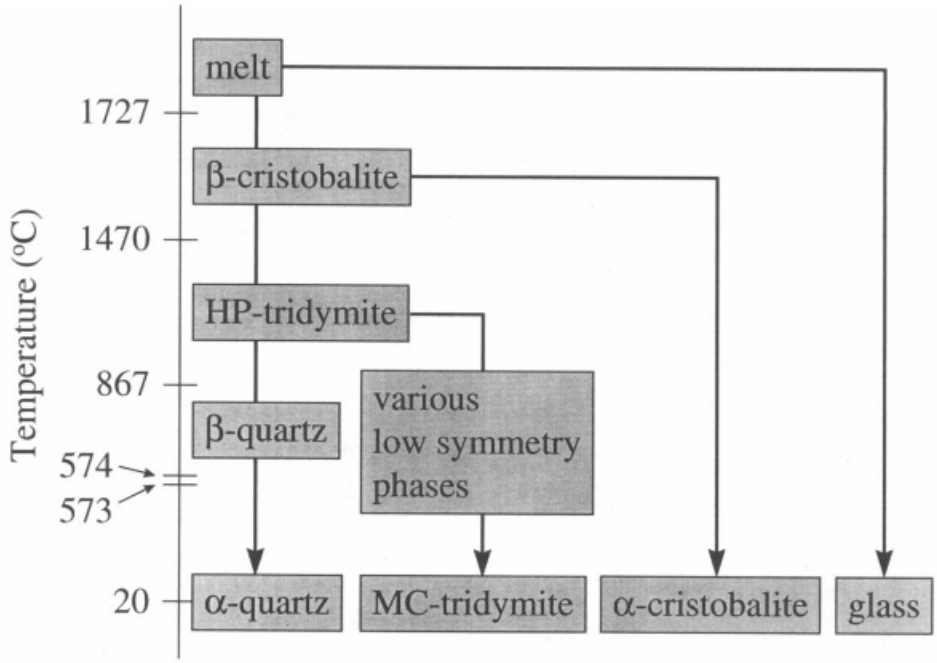

Figure 6. Schematic illustration of the various low-pressure forms of silica after Heaney[24]. The left-hand sequence from the molten phase shows the equilibrium phases whereas the other sequences show phases formed under non-equilibrium quenched conditions.

STRUCTURAL DISORDER IN CRYSTALLINE SILICAS

Introduction

Glassy silica is only one of many structural forms of SiO_2 found at ambient pressure[24]. As shown in Figure 6, at equilibrium and with decreasing temperature, the silica melt transforms in the sequence: melt → β-cristobalite → HP-tridymite → β-quartz → α-quartz. Other phases may be stabilised at room temperature with faster cooling rates: the glass (from the melt), α-cristobalite (from β-cristobalite) and MC-tridymite (from HP-tridymite, via various other low-symmetry tridymite modifications). All of these solid phases are

characterised by SiO_4 tetrahedra with differing degrees of distortion. The high temperature phases arc also believed to be significantly disordered. In the case of quartz, the thermally induced disorder results in the average crystal structure (obtained from Bragg peak intensity analysis) showing a contraction of the Si-O and O-O bond lengths accompanied by an increase in the Si-O-Si bond angle towards 180° with increased temperature (see Table 1). In β-cristobalite, the Si-O bond length is anomalously short and the Si-O-Si bond angle is 180°, with large oxygen displacement parameters normal to the Si-Si bonds[25]. A similar picture is obtained for HP-tridymite (see Figure 7). A 180° Si-O-Si bond angle is known to be unfavourable[26], and various models have been proposed to introduce disorder consistent with a more probable Si-O-Si bond angle of around 145°. One suggestion is that β-cristobalite is composed of domains of the low-temperature α-cristobalite phase[27]. Alternatively, the oxygen atoms do not lie on their average positions but instead they are dynamically distributed around this position to give a longer Si-O bond length and a more physically realistic Si-O-Si bond angle[28]. In this manner the oxygen atoms are disordered around an annulus, which may or may not contain preferred positions[29].

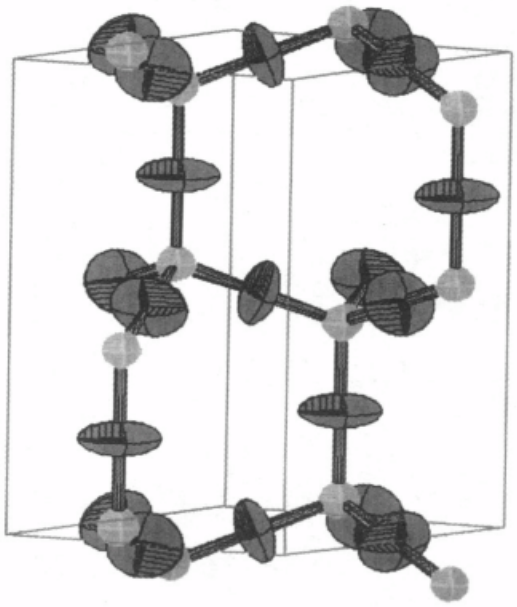

Figure 7. Average crystal structure of HP-tridymite deduced from Rietveld refinement of neutron powder data showing the SiO_4 tetrahedral units and the large anisotropic thermal ellipses of the oxygen atoms which elongate perpendicular to the Si-Si directions. [D. A. Keen and M. T. Dove (unpublished)]

In order to distinguish experimentally between possible disorder models the average structure is inappropriate. Bragg intensities arise from elastic scattering and structures deduced from them are time- and space-averaged structures. Structural disorder is then inferred from the variance in the distribution function of instantaneous atom positions that reflects the thermal motion or the partial occupancy of a number of possible sites. Such a structure would not distinguish between an average arising from a superposition of static local domains or from dynamical disorder. In contrast, total scattering directly determines local disorder. Total scattering contains the Bragg and diffuse scattering and integrates over all possible energy transfers between the probe and the sample and gives an instantaneous or 'snap-shot' picture of the structure. The *G(r)* determined from a total scattering *F(Q)* will directly determine bond lengths and can be used to distinguish between different models for structural disorder. This is demonstrated in Figure 8, which shows the low-*r* part of *rG(r)* from β-cristobalite at 300°C,[30] obtained from a direct Fourier transform

of *F(Q)* measured on the LAD neutron time-of-flight diffractometer at the ISIS spallation neutron source and compared with the positions of the shortest 'bonds' obtained from Rietveld refinement. The three lowest-*r* peaks in *G(r)* directly correspond to the Si-O, O-O and Si-Si bond lengths and can be used to deduce the O-Si-O intra- and Si-O-Si inter-tetrahedral angles. These are also shown in Table 1. It should be pointed out that time-of-flight neutron diffraction is unrivalled in this regard. A time-of-flight neutron diffractometer optimised for the study of disordered materials will measure *F(Q)* up to *Q*-values of at least 50Å^{-1} (giving good real space resolution in *G(r)* of order $2\pi/Q_{max}$) and will simultaneously determine the Bragg intensities with good *Q*-space resolution for reliable Rietveld refinement. The data shown in each column of Table 1 are from a single measurement on LAD.

Table 1. Local structural parameters of various phases of silica. Values which are not in parentheses are from Rietveld refinement of Bragg intensities. Values which are italicised and in round brackets are from the positions of the lowest-*r* peaks in *G(r)* obtained from the direct transform of *F(Q)*. ρ is the number of atoms per Å^3. Where the Rietveld refinement gives more than one bond length or angle the range of values are shown [D. A. Keen and M. T. Dove (unpublished)].

	Quartz			Cristobalite		Tridymite	Glass
T/°C(phase)	**25(α)**	**500(α)**	**620(β)**	**200(α)**	**300(β)**	**550(HP)**	**25**
ρ(Å^{-3})	0.0795	0.0773	0.0761	0.0692	0.0661	0.0655	0.0657
Si-Si (Å)	3.059 *(3.06)*	3.081 *(3.11)*	3.093 *(3.12)*	3.077 *(3.08)*	3.089 *(3.11)*	3.068/3.109 *(3.10)*	 *(3.10)*
Si-O (Å)	1.609 *(1.609)*	1.602 *(1.612)*	1.588 *(1.613)*	1.597 *(1.606)*	1.544 *(1.606)*	1.534/1.555 *(1.613)*	 *(1.617)*
O-O (Å)	2.616-2.645 *(2.632)*	2.601-2.628 *(2.626)*	2.565-2.611 *(2.627)*	2.590-2.636 *(2.623)*	2.522 *(2.623)*	2.532 *(2.634)*	 *(2.626)*
O-Si-O (°)	108.7-110.5 *(109.8)*	108.4-110.3 *(109.1)*	107.8-110.6 *(109.0)*	108.3-111.2 *(109.5)*	109.5 *(109.5)*	108.8/110.1 *(109.5)*	 *(108.6)*
Si-O-Si (°)	143.7 *(144)*	148.5 *(149)*	153.9 *(151)*	148.9 *(147)*	180.0 *(151)*	180.0 *(148)*	 *(147)*

The data from *G(r)* in Table 1 give a very different picture of the local structure of these silica phases. There is no contraction of the Si-O and O-O bond lengths and no anomalous increase in Si-O-Si bond angles towards 180° with increasing temperature. The local structure is much more physically sensible, and incidentally, much more similar to the glass.

RMC Refinement of Cristobalite

In order to characterise the structural disorder in these systems further, a structural model must be determined which is consistent with the local structure (from *G(r)*) and the average structure (from Rietveld refinement of Bragg intensities). This is an obvious

application for RMC refinement since a good starting model is available (the average structure) and RMC modelling will introduce structural disorder into the model in an unbiased manner. The procedure for refinement is as follows:

1. Use the Rietveld method to refine the Bragg peak intensities to obtain the average structure.

2. A configuration based on the ideal average structure is constructed. This may be viewed as a supercell of the crystal unit cell (e.g. 10x10x10 unit cells) and takes no account of the distribution of atoms implied from the thermal parameters in the average structure.

3. The atoms are then moved randomly one at a time so as to satisfy the constraints of Equation 10, without any comparison to *F(Q)* (i.e. $\sigma_{data}=\infty$). $R_{Si\text{-}O}$ in Equation 10 is determined from the lowest-*r* peak in *G(r)*. $\sigma_{Si\text{-}O}$ and $\sigma_{O\text{-}Si\text{-}O}$ are chosen to approximately reproduce the widths of the two lowest-*r* peaks in *G(r)*. The atom-atom connectivity is maintained throughout.

4. The weighting of fit to *F(Q)* is slowly increased (σ_{data} is slowly decreased) with respect to the constraints until a good fit to the data is obtained.

The constraints are not too strong to dominate the final structure but are necessary to impose SiO_4 tetrahedra on the structure during the RMC refinement. Indeed the final refined model has broader Si-O and O-O peaks in *G(r)* and a broader O-Si-O bond angle distribution than would be expected on the basis of the constraints alone.

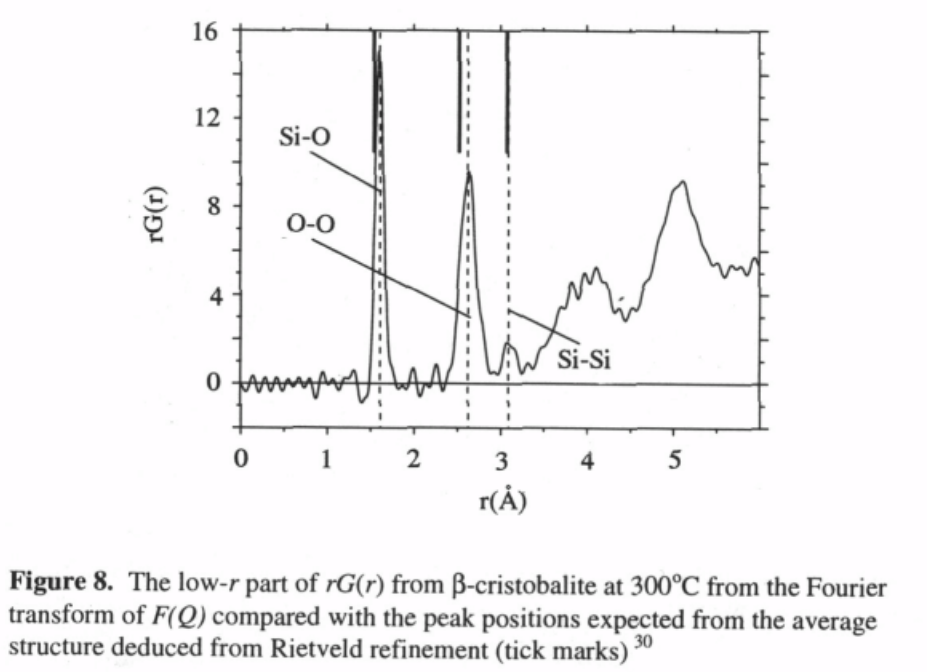

Figure 8. The low-*r* part of *rG(r)* from β-cristobalite at 300°C from the Fourier transform of *F(Q)* compared with the peak positions expected from the average structure deduced from Rietveld refinement (tick marks) [30]

The crystalline long-range order must be effectively accounted for in the model. It is only possible to calculate *G(r)* from the model out to distances $L_{min}/2$, where L_{min} is the shortest dimension of the configuration box. This is equivalent to the perfect long-range *G(r)* ($0<r<\infty$) multiplied by a step function *m(r)* where $m(r)=1$ if $m(r)<L_{min}/2$ and $m(r)=0$ otherwise. The Fourier transform of this section of *G(r)* is *F(Q)* convoluted with the transform of *m(r)*, i.e. $M(Q)=\sin(QL_{min}/2)/Q$. This has the effect of broadening the sharp

Bragg peaks and comparison between $F_{expt}(Q)$ and the calculated $F_{calc}(Q)$ from the configuration would be inappropriate. Hence the comparison is made between $F_{calc}(Q)$ and $F_{expt}(Q)$ convoluted with $M(Q)$, i.e. $F(Q)^L$

$$F^L_{expt}(Q_j) = \frac{1}{\pi}\int F_{expt}(Q_t)\left(\frac{\sin(|Q_t - Q_j|L/2)}{|Q_t - Q_j|} - \frac{\sin(|Q_t + Q_j|L/2)}{|Q_t + Q_j|}\right)dQ_t \qquad (11)$$

This procedure is not usually necessary for glassy or liquid data where $G(r)$ is flat at $r=L_{min}/2$. The alternative to this is to compare $G_{calc}(r)$ with $G_{expt}(r)$ where $G_{expt}(r)$ has been determined using an inverse method which bypasses the truncation effects of the forward transform $F(Q)\rightarrow G(r)$ when $F(Q)$ is not flat at the maximum Q measured. Such techniques will not be described here, and readers are referred to Soper *et al*[31].

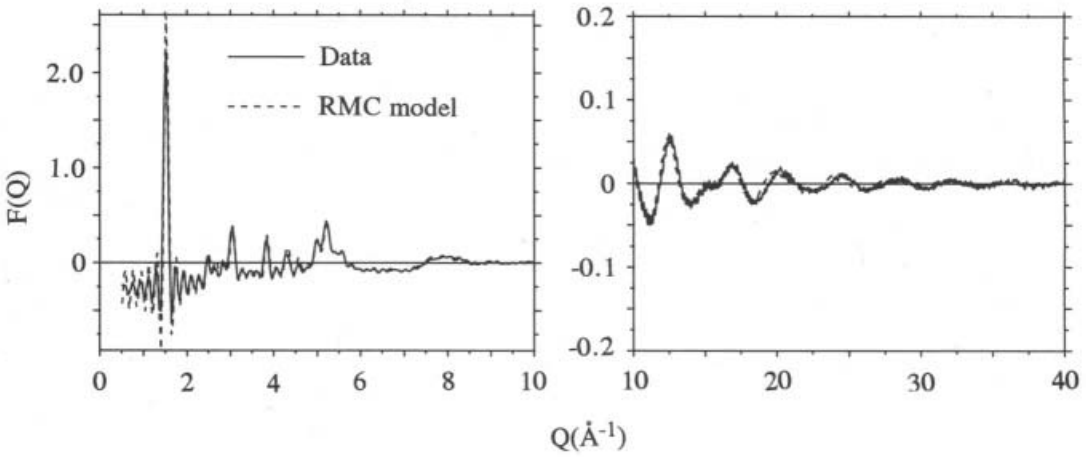

Figure 9. Structure factor of β-cristobalite at 300°C convoluted with the Fourier transform of an appropriate sized step function (full line) (see text for details) and compared with the structure factor from the RMC refined model (dashed line). Note the change of scales between the left-hand (low-Q) and right-hand (high-Q) panels.

The RMC fit to the $F(Q)$ data from β-cristobalite at 300°C is shown in Figure 9. The model consisted of 24,000 atoms (10x10x10 unit cells within a cubic box of sides L=71.351Å). The initial model was created by placing the atoms on the positions determined from Rietveld refinement of the data and then randomly moving atoms to increase the Si-O distance from the Rietveld determined value of 1.544Å to the bond length determined from the lowest-r peak in $G(r)$ (1.606Å) while maintaining the tetrahedral SiO_4 arrangement, using constraints described by Equation 10. This starting model was then refined using the $F(Q)$ data and the RMC method described at the start of this section. Figure 10 shows the comparison between $rG(r)$ calculated from the RMC model and $rG(r)$ obtained from the direct transform of $F(Q)$. This shows that very good agreement is also obtained between the real space correlation functions. The bond-angle distribution functions are shown in Figure 11 and the partial radial distribution functions in Figure 12. Three things should be noted. First, as discussed previously[30] the $G(r)$ for β-cristobalite is similar to that of the glass and different from α-cristobalite. This would discount the suggestion that β-cristobalite is an average of α-cristobalite domains. Secondly, the distribution of O around the bond-joining neighbouring Si atoms in [111] directions is isotropic in θ (the torsional angle around the Si-Si bond) and peaks at $\phi \sim 17^o$ (the angle

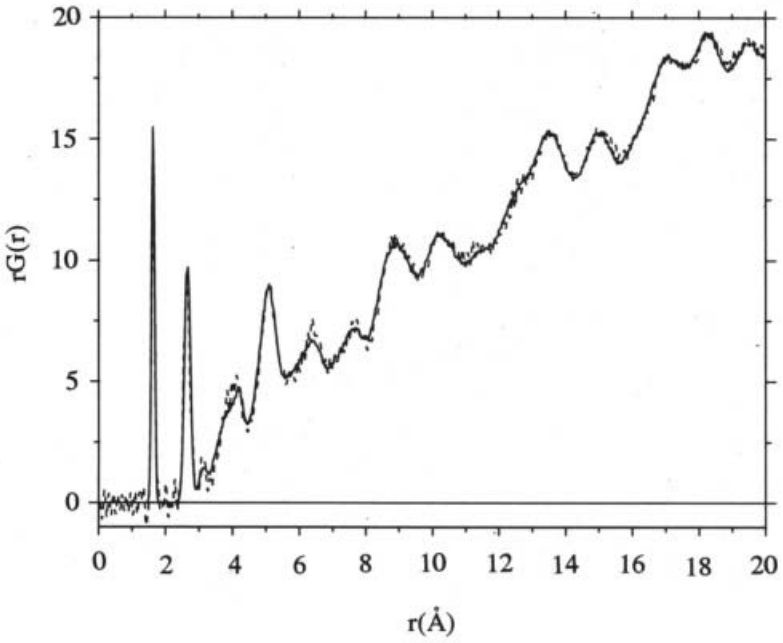

Figure 10. $rG(r)$ from β-cristobalite at 300°C from the Fourier transform of the experimental $F(Q)$ (dashed line) compared with the same function from the model produced from RMC refinement (full line).

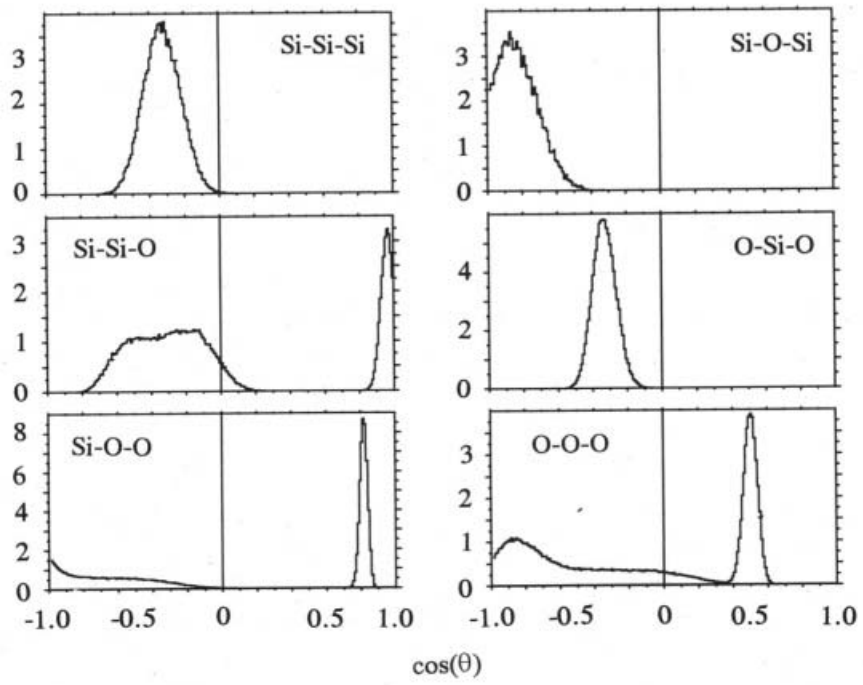

Figure 11. Nearest neighbour bond angle distributions for β-cristobalite at 300°C calculated from the RMC refined model (arbitrary units).

between the Si-O bond and the Si-Si direction). Hence there is no evidence for preferred oxygen sites on this ring of O density in the RMC model. Thirdly, it is possible to use the RMC model to calculate the expected diffuse scattering in planes of reciprocal space. This is equivalent to the scattering which would be measured from a single crystal (if one existed that were large enough) and the calculation is possible because of the three-dimensional nature of the RMC model. The diffuse scattering in the (hk0) plane is shown in Figure 13 and compared with electron diffraction results from a very small single crystal grain[32]. There is very good agreement in the positions of the diffuse scattering lines which occur principally in 110 and 100 directions in this plane. This shows that the RMC model

is not only able to reproduce the one dimensional *F(Q)* but also three-dimensional scattering data. Further discussion of the results from these models, and similar models of other phases of crystalline silica will be presented in a later paper[33], although some of the consequences of these models on rigid unit mode theories of silicate minerals are described in another chapter of this book by M. T. Dove *et al.*

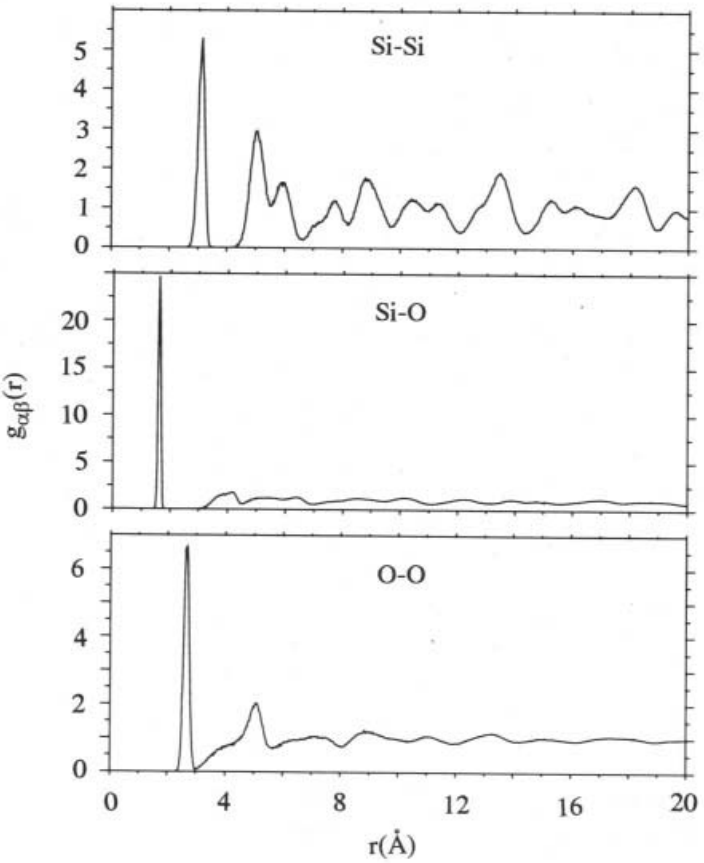

Figure 12. Partial radial distribution functions $g_{\alpha\beta}(r)$ for β-cristobalite at 300°C calculated from the RMC refined model.

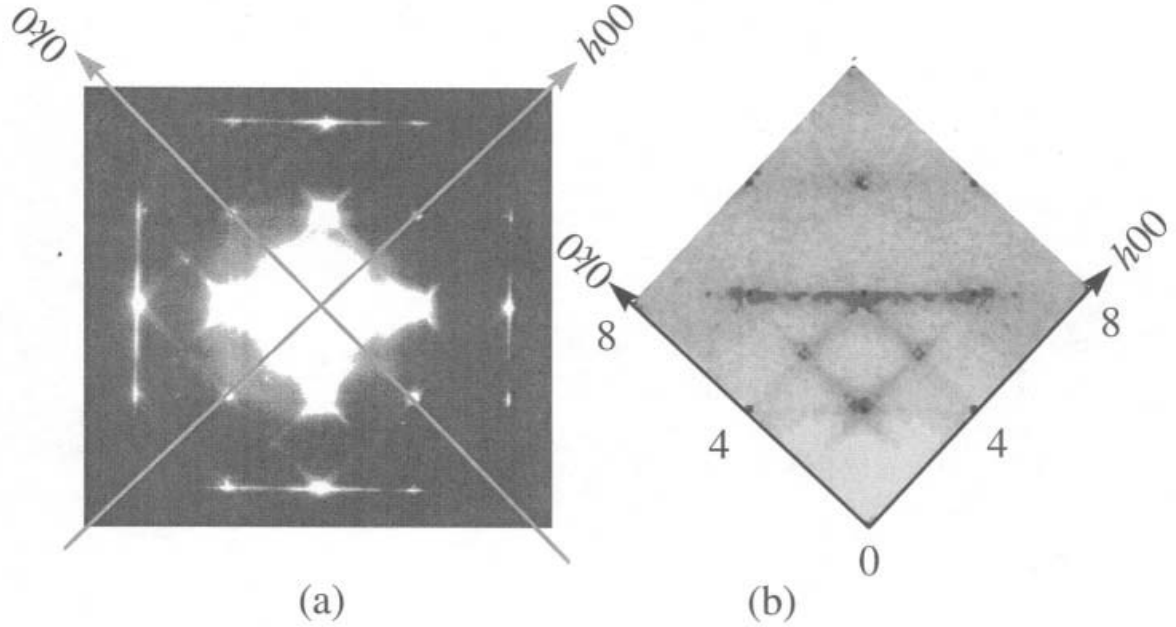

Figure 13. Diffuse scattering from β-cristobalite in the *hk*0 reciprocal lattice plane. (a) measured by electron diffraction[32] and (b) from the RMC refined model.

CONCLUSIONS

This chapter has described in detail the techniques of RMC modelling and refinement. Results from glassy silica and the disordered crystalline β-phase of cristobalite have been presented. These results show that with careful application of RMC methods, good representative structures of both locally ordered glasses and locally disordered crystals can be obtained. These methods are completely general and can be applied successfully to a wide range of systems which show structural disorder, with careful consideration to the form of constraints and the construction of appropriate starting models.

Acknowledgements

I am extremely grateful to Martin Dove who has collaborated with me on the study of local disorder in crystalline silica phases and who has permitted me to quote some of our results here prior to full publication. I also thank Jim Wicks for helpful discussions about the structure of glassy silica and the use of some of his unpublished results and Richard Welberry for providing me with the electron diffraction result shown in Figure 13.

REFERENCES

1. M.A. Howe, R.L. McGreevy and W.S. Howells, J. *Phys: Condensed Matter* 1:3433 (1989)
2. T.E. Faber and J.M. Ziman, *Phil. Mag.* 11:153 (1965)
3. R. Kaplow, T.A. Rowe and B.L. Averbach, *Phys. Rev.* 168:1068 (1968)
4. M.D. Rechtin, A.L. Renninger and B.L. Averbach, *J. Non-Cryst. Sol.* 15:74 (1974)
5. R.L. McGreevy and L. Pusztai, *Mol. Sim.* 1:359 (1988)
6. R.L. McGreevy, *Nucl. Instr. and Meth.* A 354:1 (1995)
7. R.A. Young (ed.), *The Rietveld Method* International Union of Crystallography, Oxford University Press, Oxford (1995)
8. N. Metropolis, A.W. Rosenbluth, M.N. Rosenbluth, A.H. Teller and E. Teller, *J. Chem. Phys.* 21:1087(1953)
9. K. Binder and D.W. Heermann. *Monte Carlo Simulation in Statistical Physics - An Introduction,* (2^{nd} edition) Springer-Verlag, Berlin (1992)
10. J.E. Enderby and G.W. Nielson, *Rep. Prog. Phys.* 44:593 (1981)
11. W.H. Zachariasen, *J. Am. Chem. Soc.* 54:3841 (1932)
12. D.I. Grimley, A.C. Wright and R.N. Sinclair, *J. Non-Cryst. Sol.* 119:49 (1990)
13. E. Dupree and R.F. Pettifer, *Nature* 308:523 (1984)
14. H.F. Poulsen, J. Neuefeind, H.-B. Neumann, J.R. Schneider and M.D. Zeidler, *J. Non-Cryst. Sol.* 188:63 (1995)
15. R.J. Bell and P. Dean, *Nature* 212:1354 (1966)
16. L.F. Gladden, *J. Non-Cryst. Sol.* 119:318 (1990)
17. J.D. Kubicki and A.C. Lasaga.Am. *Min.* 73:941 (1988); B. Vessal, M. Amini and C.R.A. Catlow, *J. Non-Cryst. Sol.* 159:184 (1993); J. Sarnthein, A. Pasquarello and R. Car, *Phys. Rev.* B 52:12690 (1995)
18. D.A. Keen and R.L. McGreevy, *Nature* 344:423 (1990)
19. J.D. Wicks, D.Phil Thesis, Oxford (1993)
20. R.L. Mozzi and B.E. Warren, *J. Appl. Cryst.* 2:164 (1969)
21. D.A. Keen, *Phase Transitions* 61:109 (1997)
22. L.F. Gladden, in: *The Physics of Non-crystalline Solids,* eds. L.D. Pye, V.C. Lacourse and H.J. Stevens, Taylor and Francis, London (1992)

23. M. Bionducci, F. Buffa, G. Licheri, A. Musinu, G. Navarra and G. Piccaluga, *J. Non-Cryst. Sol.* 177:137 (1994)
24. P.J. Heaney, *Reviews in Mineralogy* 29:1 (1994)
25. W.W. Schmahl, I.P. Swainson, M.T. Dove and A. Graeme-Barber, Z. *Kristallogr.* 201:125(1992)
26. G.V. Gibbs, E.P. Meagher, M.D. Newton and D.K. Swanson, in: *Structure and Bonding in Crystals,* eds. M. O'Keeffe and A. Navrotsky, Academic Press, New York (pages 195-225) (1981)
27. D.M. Hatch and S. Ghose, *Phys. Chem. Minerals* 17:554 (1991)
28. I.P. Swainson and M.T. Dove, *Phys. Rev. Lett.* 71:193 (1993)
29. T.R. Welberry, G.L. Hua and R.L. Withers, *J. Appl. Cryst.* 22:87 (1989)
30. M.T. Dove, D.A. Keen, A.C. Hannon and I.P. Swainson, *Phys. Chem. Minerals* 24:311 (1997)
31. A.K. Soper, C. Andreani and M. Nardone, *Phys. Rev.* E 47:2598 (1993)
32. G.L. Hua, T.R. Welberry, R.L. Withers and J.G. Thompson, *J. Appl. Cryst. 2*1:458 (1988)
33. D.A. Keen and M.T.Dove (unpublished)